Solar and Stellar Variability: Impact on Earth and Planets
Proceedings IAU Symposium No. 264, 2009
A. G. Kosovichev, A. H. Andrei & J.-P. Rozelot, eds.

doi:10.1017/S1743921309992857

Thermospheric temperature and density variations

Hitoshi Fujiwara[1], Yasunobu Miyoshi[2], Hidekatsu Jin[3], Hiroyuki Shinagawa[4], Yuichi Otsuka[5], Akinori Saito[6] and Mamoru Ishii[7]

[1]Department of Geophysics, Tohoku University, Sendai, Japan
email: fujiwara@pat.gp.tohoku.ac.jp

[2]Department of Earth and Planetary Sciences, Kyushu University, Fukuoka Japan
email: miyoshi@geo.kyushu-u.ac.jp

[3]National Institute of Communication Technology, Tokyo, Japan
email: jin@nict.go.jp

[4]National Institute of Communication Technology, Tokyo, Japan
email: sinagawa@nict.go.jp

[5]Solar Terrestrial Environment Laboratory, Nagoya University, Nagoya, Japan
email: otsuka@ste.nagoya-u.ac.jp

[6]Department of Geophysics, Kyoto University, Kyoto, Japan
email: saitoua@kugi.kyoto-u.ac.jp

[7]National Institute of Communication Technology, Tokyo, Japan
email: mishii@nict.go.jp

Abstract. The thermosphere is the transition region from the atmosphere to space. Both the solar ultraviolet radiation and the solar wind energy inputs have caused significant thermospheric variations from past to present. In order to understand thermospheric/ionospheric disturbances in association with changes in solar activity, observational and modelling efforts have been made by many researchers. Recent satellite observations, e.g., the satellite CHAMP, have revealed mass density variations in the upper thermosphere. The thermospheric temperature, wind, and composition variations have been also investigated with general/global circulation models (GCMs) which include forcings due to the solar wind energy inputs and the lower atmospheric effects. In particular, we have developed a GCM which covers all the atmospheric regions, troposphere, stratosphere, mesosphere, and thermosphere, to describe variations of the thermospheric temperature and density caused by both effects from the lower atmosphere and the magnetosphere. GCM simulations represent global and localized temperature and density structures, which vary from hour to hour, depending on forcings due to the lower atmosphere, solar and geomagnetic activities. This modelling attempt will enable us to describe the thermospheric weather influenced by solar activity in cooperation with ground-based and satellite observations.

Keywords. solar-terrestrial relations, solar wind, sunspots

1. Introduction

The thermospheric temperature and density have been observed with satellites and ground-based optical and radar techniques. The early satellites provided thermospheric density data obtained from their orbital changes due to the air-drag force (e.g., King-Hele, 1959, 1987). The mass spectrometer measurements by satellites also have revealed composition and density changes in the thermosphere (e.g., Prölss, 1982). The accelerometer measurements by satellites have successfully described spatio-temporal variations of the thermospheric density at present. For example, the double-hump structure of the

neutral mass density in the equatorial region (Liu *et al.*, 2005), density enhancements due to traveling atmospheric disturbances (e.g., Forbes *et al.*, 2005; Bruinsma *et al.*, 2006), density enhancements during solar flare events (e.g., Sutton *et al.*, 2006) ere found from accelerometer measurements by he CHAMP satellite.

The Fabry-Perot interferometer (FPI), which can detect the Doppler shifted and broadening emissions from the atmospheric species, is one of the most important instruments to observe the neutral temperature and wind in the thermosphere (e.g., Aruliah *et al.*, 1991; Ishii *et al.*, 1999; Shiokawa *et al.*, 2003; Ford *et al.*, 2007). In addition, the radar techniques enable us to obtain information of the thermospheric wind and temperature. The lower thermospheric wind and temperature and the exospheric temperature have been obtained from the incoherent scatter (IS) radar observations (e.g., Nozawa and Brekke, 1995; Buonsanto *et al.*, 1998).

The global numerical models, which are so-called general/global circulation models (GCMs), of the thermosphere have been developed since the first one by Fuller-Rowell and Rees (1980). Recently, the GCMs have become ones which are coupled with models of the ionosphere, magnetosphere, and the lower atmosphere (e.g., Roble, 2000; Miyoshi and Fujiwara, 2003, 2009; Wang *et al.*, 2004; Toth *et al.*, 2007; Akmaev *et al.*, 2008; Fuller-Rowell *et al.*, 2008). These models are now essential for space weather researches to understand effects of the solar activity on the geospace environment.

The global (large-scale) patterns of the thermospheric wind, temperature, and density during both the solar minimum and maximum periods are almost understood from the observational and modelling studies as mentioned above. Some empirical (statistical) models have been developed based mainly on the ground-based radar and optical observations and satellite and rocket observations. The standard ones are, for example, NRLMSISE-00 (Picone *et al.*, 2002) for the thermospheric temperature and composition (density), HWM (Hedin *et al.*, 1996) for the thermospheric wind, and International Reference Ionosphere (IRI) (Bilitza and Reinisch, 2008) for the ionospheric parameters (ion temperature and composition, electron temperature and density).

Although the empirical models describe well the global patterns of the thermospheric temperature and density depending on the 11-year solar cycle, there are some discrepancies between the localized structures obtained from observations and the empirical models. It is also difficult to describe disturbances of the thermosphere during geomagnetic storms by using the empirical models and GCMs. In addition, previous GCMs cannot predict day-to-day variations of the thermosphere and ionosphere even during geomagnetically quiet periods. In order to understand the above unknown features of the thermosphere, we have developed a GCM which covers all the atmospheric regions, troposphere, stratosphere, mesosphere, and thermosphere. The GCM calculates the thermospheric temperature, density, and wind varying from hour to hour. The thermospheric temperature and density variations due to the solar external forcing and the lower atmospheric effects simulated by the GCM are shown in the following sections.

2. Basic features of the thermospheric temperature and density

The thermospheric temperature and density profiles are determined primarily by the solar energy inputs into the thermosphere. The height of the thermospheric upper boundary also depends on the solar energy inputs; namely, the height depends on the solar and geomagnetic activities, local time, latitude, and season. The temperature profiles obtained from an empirical model of NRLMSISE-00 are shown in Figure 1. The solid and dashed lines indicate the temperatures during the periods of the solar minimum in winter and the solar maximum in summer, respectively. These are the typical ones at mid-latitude at

https://doi.org/10.1017/S1743921309992857 Published online by Cambridge University Press

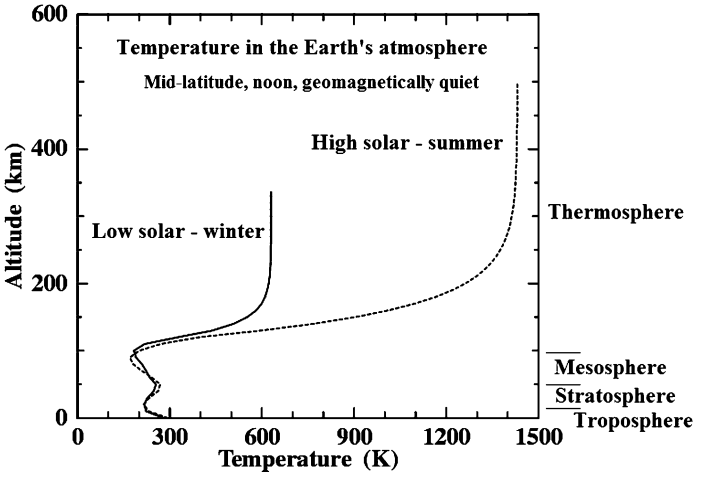

Figure 1. Examples of the temperature profiles obtained from an empirical model of NRLMSISE-00 for solar minimum and maximum conditions at mid-latitude noon.

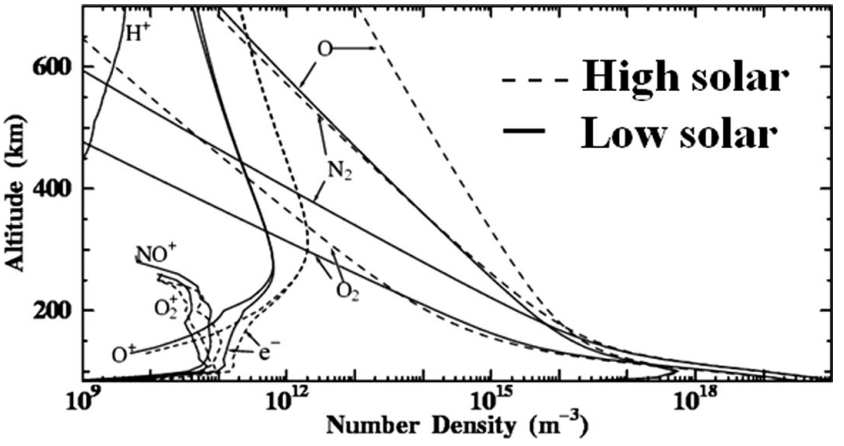

Figure 2. Height profiles of the major constituents in the thermosphere and ionosphere obtained from empirical models of NRLMSISE-00 and IRI for solar minimum and maximum conditions at mid-latitude noon.

noon for geomagnetically quiet condition. In the above case, the temperature at the top of the thermosphere (i.e., the exospheric temperature) changes by about 800 K due to the 11-year solar cycle since the atmospheric species obtain their thermal energy mainly from the solar extreme ultraviolet (EUV) and ultraviolet (UV) radiation which strongly depends on the solar activity.

Figure 2 shows height profiles of the major constituents in the thermosphere and ionosphere obtained from empirical models of NRLMSISE-00 and IRI. The solid and dashed lines indicate profiles during the solar minimum and maximum periods, respectively. These profiles are also typical ones at mid-latitude at noon for geomagnetically quiet condition. The neutral species show significant enhancements at high altitudes during the solar maximum period due to thermal expansion of the air or increase in the scale-height. For example, the number densities of the atomic oxygen and molecular nitrogen at 400 km altitude vary more than one order during the 11-year solar cycle in this case.

https://doi.org/10.1017/S1743921309992857 Published online by Cambridge University Press

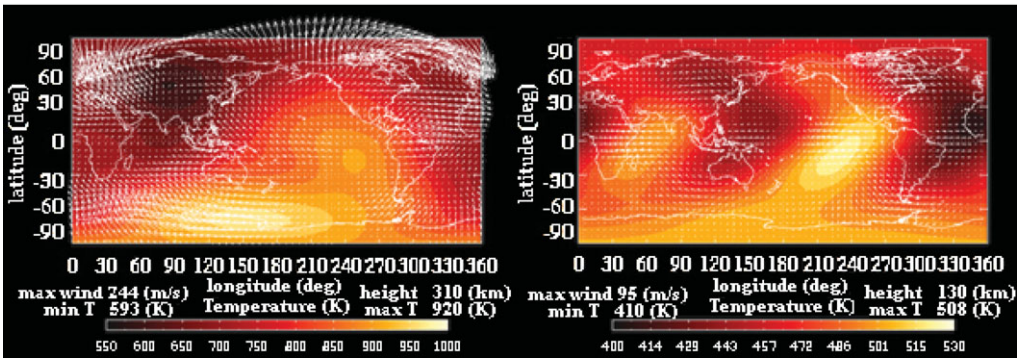

Figure 3. The global distributions of the thermospheric temperature and wind obtained from empirical models of NRLMSISE-00 and HWM in December during the solar minimum and geomagnetically quiet period at 310 (left panel) and 130 km (right panel) altitudes. Note that the strength of wind vector and temperature range are different in each panel.

The global distributions of the thermospheric temperature and wind obtained from empirical models of NRLMSISE-00 and HWM are shown in Figure 3. The left and right panels indicate the global distributions in December during the solar minimum and geomagnetically quiet period at 310 and 130 km altitudes, respectively. The maximum wind vector indicates 244 and 95 m/s in the left and right panels, respectively. At 310 km altitude (left panel), diurnal temperature distribution is remarkable. In addition, high temperature region is clearly seen in the southern (summer) hemisphere. At 130 km altitude (right panel), semi-diurnal temperature variation is clear in the low-latitude region. High temperature regions are also seen at high-latitudes, particularly in the southern (summer) hemisphere.

3. Whole atmosphere GCM

In the present study, we use a whole atmosphere GCM developed by Miyoshi and Fujiwara (2003) as an extension of the middle atmosphere GCM developed at Kyushu University (Miyahara *et al.*, 1993; Miyoshi, 1999). The GCM was originally developed as a tropospheric GCM at the Japan Meteorological Agency (Kanamitsu *et al.*, 1983), and developed as a community climate model at the University of Tokyo. The GCM was extended to include the processes of the middle atmosphere, and then the thermosphere.

The whole atmosphere GCM solves the full nonlinear primitive equations for momentum, thermodynamics, continuity, and hydrostatics. The continuity equation of mass mixing ratio for the major species, N_2, O_2, and O, is also solved taking into account the photo-dissociation of O_2 and oxygen chemistry. The EUVAC spectral model (Richards *et al.*, 1994) is used for the solar EUV flux poured into the thermosphere. This GCM is a global spectral model (triangular truncation of T21 which is equivalent to a spatial resolution of 5.6^o for latitude and longitude) with 75 vertical pressure levels (vertical resolution of 0.4 scale height above the tropopause) and contains all the atmospheric regions from the ground to exobase. The time step for integrating the equations is 100 s. The corrected centered dipole is assumed to describe the Earth's magnetic field. The effects of auroral particle precipitation on heating the neutral gases are evaluated by using an analytical prescription into the auroral oval. The magnetospheric convection electric field and empirical ionosphere are used for calculating Joule heating and ion-drag force. The details of the GCM are described in Miyoshi and Fujiwara (2003, 2006), Fujiwara and Miyoshi (2006), and references therein.

https://doi.org/10.1017/S1743921309992857 Published online by Cambridge University Press

4. Thermospheric temperature and density variations simulated by GCM

Figure 4 shows GCM results of global temperature and horizontal wind distributions at 00:00 UT on March 5, June 5, September 5, and December 5 on a constant-pressure surface of about 302-312 km altitude. Note that the strength of the maximum wind vector is different in each panel to overview global wind patterns. Diurnal (or day-night) temperature variation is clearly seen in all the panels. In the December case, the large-scale (day-night) temperature structure is quite similar to that from an empirical model of NRLMSISE-00 shown in Figure 3; namely, high temperature regions at dayside low-latitudes and southern (summer) high-latitudes. On the other hand, localized temperature structures appear in the simulation results; for example, localized structures are clearly seen from high- to low-latitudes in the southern (summer) hemisphere in the December case. Fujiwara and Miyoshi (2009) showed that the localized structures resulted from the lower atmospheric effects which cause day-to-day variation of the thermospheric temperature. Some localized structures in the simulation results show wavy structures/variations. For example, wavy structures are seen at around the solar terminator and auroral oval. Fujiwara and Miyoshi (2006) made mention of these structures based on their GCM simulations as one of characteristics of the thermospheric temperature structure during geomagnetically quiet periods.

Figure 5 shows GCM results of global density distributions at 00:00 UT on March 5, June 5, September 5, and December 5 at a specific height of 400 km. Although the atmospheric parameters are calculated on constant pressure surfaces because of assumption of the hydrostatics, we can infer the parameters at a specific height from the output data with the spline interpolation. The density variation ranges are 0.93-3.56 $\times$ 10^{-12} kg/m^3, 1.02-4.22 $\times$ 10^{-12} kg/m^3, 0.84-3.47 $\times$ 10^{-12} kg/m^3, and 1.12-4.44 $\times$ 10^{-12} kg/m^3 in March, June, September, and December, respectively. Localized/wavy structures are also seen in the high-latitude region and near solar terminator particularly in the June and December cases. Forbes *et al.* (2008) found solar terminator waves from the neutral mass density variations observed by CHAMP. These waves are closely related to tidal forcings originating from the lower atmosphere (Miyoshi *et al.*, 2009).

Sudden changes in the energy inputs into the thermosphere due to the solar wind variation produce high temperature (pressure) regions at high-latitude. The produced pressure bulges generate traveling atmospheric disturbances (TADs) which propagate globally in the thermosphere. Figure 6 shows examples of TADs simulated with the whole atmosphere GCM. In this case, the cross polar cap potential drop is changed from 30 (initial level) to 60 kV (disturbed level) during 1-hour (00:00-01:00 UT) to produce TADs. The upper panel shows usual simulation results for the thermospheric temperature and wind at 00:00 UT on December 1 on a constant pressure surface of about 310 km altitude. The middle panel shows temperature and wind distributions at 100 minutes after enhancement of the high-latitude energy inputs. High temperature regions, which extend almost in the longitudinal direction, are clearly seen from high- to mid-latitudes. The bottom panel shows differences of temperature and wind between results with TADs (middle panel) and in the usual case. Longitudinally-extent TADs, which are generated and propagate from high- to low-latitudes, are clearly seen in both hemispheres in the bottom panel. Fujiwara and Miyoshi (2006, 2009) also performed TAD simulations with the whole atmosphere GCM. Superposition of TADs and the lower atmospheric effects can produce localized temperature structures globally in the upper thermosphere (Fujiwara and Miyoshi, 2009). Figure 6 also shows localized temperature structures produced by TADs and the lower atmospheric effects. In this case, the amplitudes of TADs are in the

https://doi.org/10.1017/S1743921309992857 Published online by Cambridge University Press

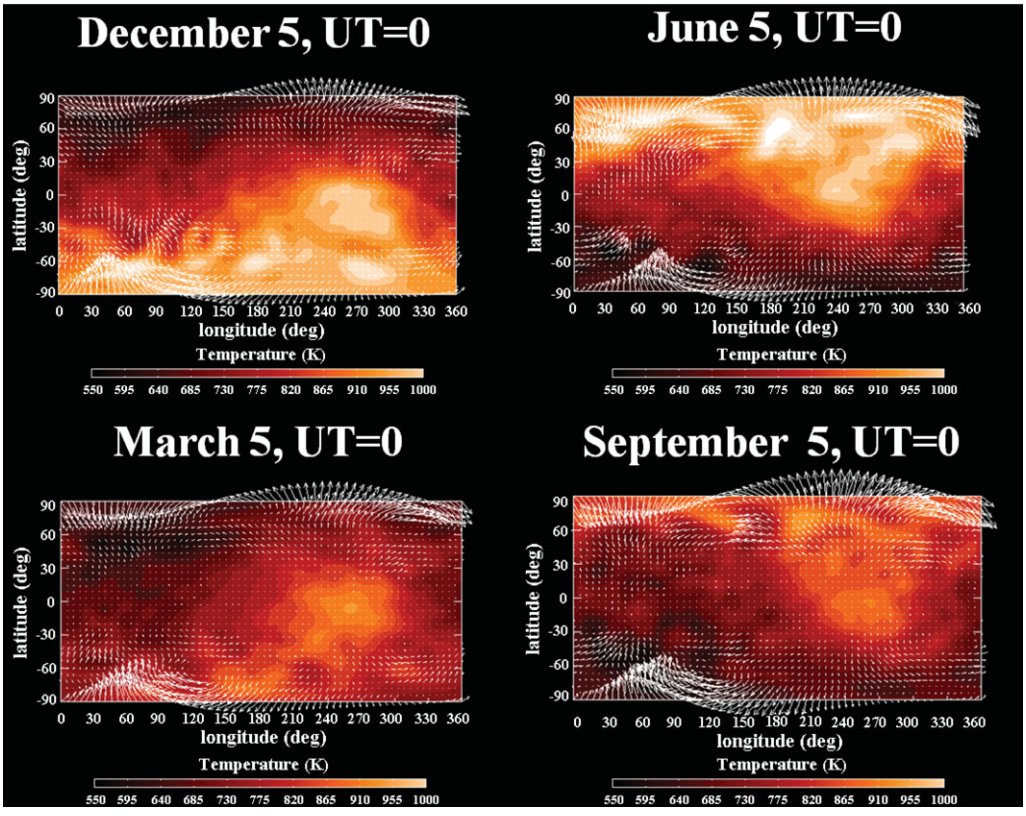

Figure 4. GCM results of temperature and horizontal wind distributions at 00:00 UT on March 5, June 5, September 5, and December 5 on a constant-pressure surface of about 302-312 km altitude. Note that the strength of the maximum wind vector is different in each panel to overview global wind patterns.

temperature range between -50 and 133 K. In addition to TADs propagating from high- to low-latitudes, TADs propagating over the polar cap region are seen in the dayside and nightside regions in the northern and southern hemispheres, respectively (see bottom panel).

5. Future works

In addition to the thermospheric phenomena, the ionospheric ones and coupling processes between the thermospheric neutrals and ionospheric plasmas are quite interesting. Recent observations have revealed ionospheric variations originating from the tropospheric phenomena (e.g., "Coupling Processes in the Equatorial Atmosphere" the special issue of Earth Planets and Space, vol.61(No.4), 2009). In order to describe the coupling results, we have started a modelling study for coupling the whole atmosphere GCM and ionospheric models. As the first step of the work, we investigated low-latitude ionospheric variations (e.g., wavenumber-4 structure) caused by the atmospheric tidal forcings by using an ionospheric dynamo model with use of the GCM output data (Jin *et al.*, 2008).

Some projects for the thermospheric/ionospheric sciences are planned in the Japanese community. For example, our future satellite mission, the Ionosphere, Mesosphere, upper Atmosphere, and Plasmasphere mapping (IMAP), will provide us with important information on coupling between the ionosphere and atmosphere through optical imaging

https://doi.org/10.1017/S1743921309992857 Published online by Cambridge University Press

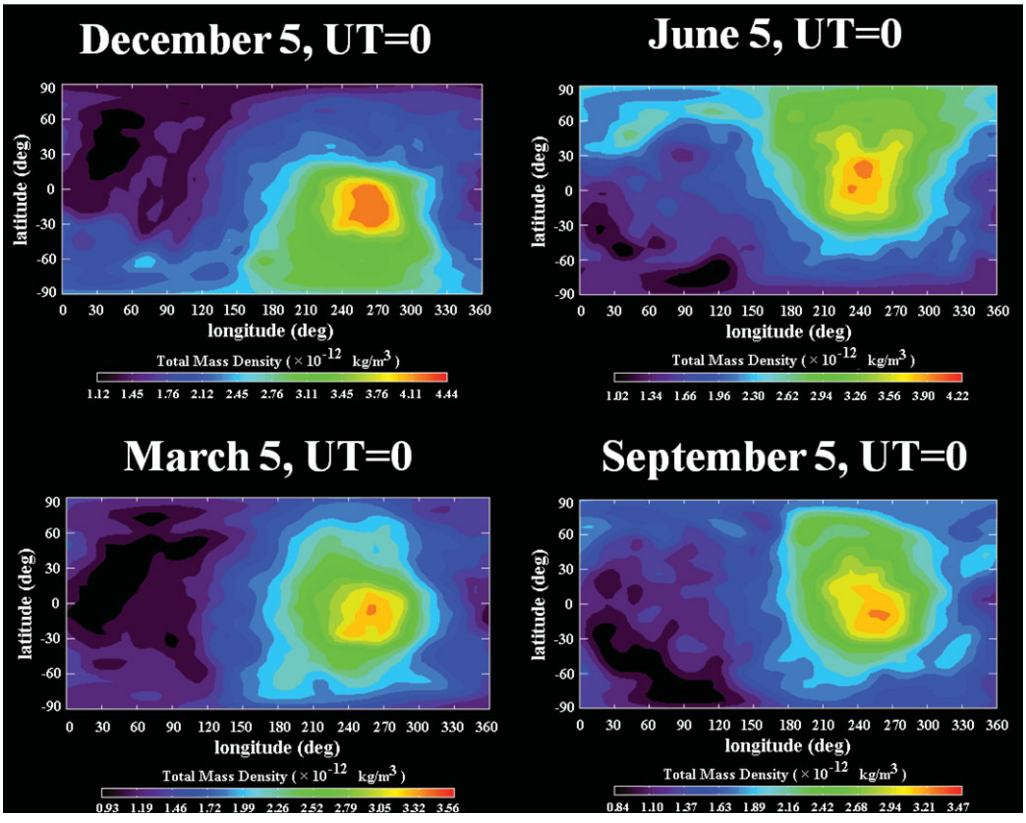

Figure 5. Same as Figure 4 except for neutral mass density at a specific height of 400 km.

observations. The IMAP project is now moving ahead as one of application projects of International Space Station (ISS).

6. Summary

The thermospheric temperature and density variations have been investigated from observational and modelling studies. The general features of thermospheric responses to change in the solar activity due to the 11-year solar cycle have been well understood. However, thermospheric localized structures and their variations from hour to hour are not understood well. In addition, it is also difficult to describe thermospheric responses to sudden changes in the solar radiation and solar wind energy inputs. Modelling efforts of the Earth's and planetary atmospheres are essential to understanding the solar variability impacts on Earth and planets. In particular, general/global circulation model (GCM), which includes all the atmospheric regions, is a very effective tool for studying coupling processes between the lower and upper atmospheres. Our whole atmosphere GCM simulates the thermospheric variations from hour to hour, localized wavy structures, and traveling atmospheric disturbances. The future coupled model of the whole atmosphere and the ionosphere will describe more details of the coupling phenomena between the thermospheric neutrals and the ionospheric plasmas in cooperation with ground-based observations and future missions, e.g., the IMAP project in Japan.

https://doi.org/10.1017/S1743921309992857 Published online by Cambridge University Press

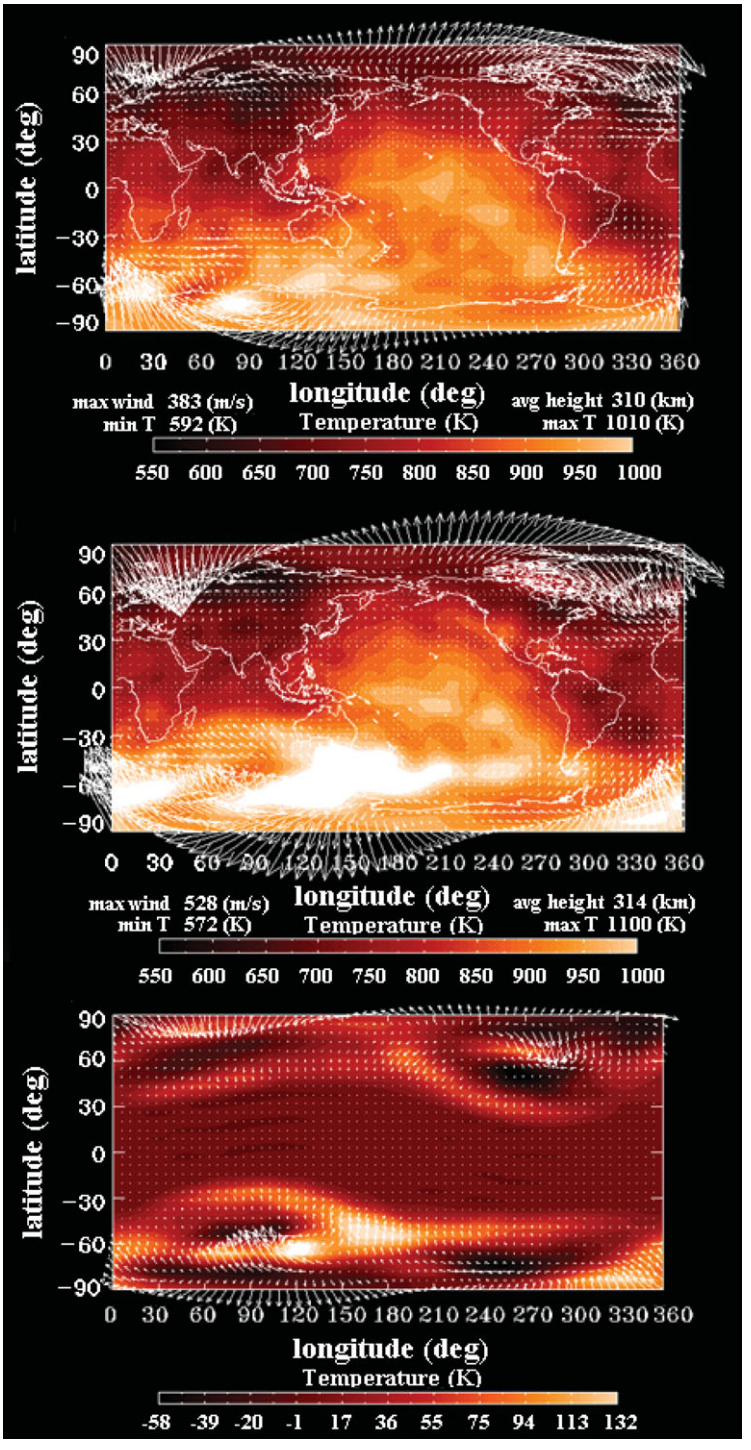

Figure 6. The thermospheric temperature and wind at 00:00 UT on December 1 on a constant pressure surface of about 310 km altitude obtained from GCM simulation in the same condition as that shown in Figure 4 (upper panel). Temperature and wind distributions at 100 minutes after enhancement of the high-latitude energy inputs (middle panel). Differences of temperature and wind between results of usual and TADs simulations (bottom panel). (See text for details)

https://doi.org/10.1017/S1743921309992857 Published online by Cambridge University Press

Acknowledgements

This work was supported in part by Grant-in-Aid for Scientific Research C (20540435), Grant-in-Aid for Scientific Research on Innovative Areas (20200047), and the Global COE program "Global Education and Research Center for Earth and Planetary Dynamics" at Tohoku University by the Ministry of Education, Science, Sports and Culture, Japan. A part of this work was also supported by the joint research program of the Solar-Terrestrial Environment Laboratory, Nagoya University. The empirical models of NRLMSISE-00 and HWM-93 are provided by NSSDC/NASA and IRI is from ModelWeb of CCMC/NASA.

References

Akmaev, R. A., Fuller-Rowell, T. J., Wu, F., Forbes, J. M., Zhang, X., Anghel, A. F., Iredell, M. D., Moorthi, S., & Juang, H.-M. 2008, *Geophys. Res. Lett.*, 35, L03810, doi:10.1029/2007GL032584.

Aruliah, A. L., Fuller-Rowell, T. J., and Rees, D. 1991, *J. Atmos. Terr. Phys.*, 53, 467.

Bilitza, D. & Reinisch, B. 2008, *J. Adv. Space Res.*, 42, 599.

Bruinsma, S., Forbes, J. M., Nerem, R. S., & Zhang, X. 2006, *J. Geophys. Res.*, 111, A06303, doi:10.1029/2005JA011284.

Buonsanto, M. J. & Pohlman, L. M. 1998, *J. Geophys. Res.*, 103 , 23381.

Forbes, J. M., Lu, G., Bruinsma, S., Nerem, R. S., & Zhang, X. 2005, *J. Geophys. Res.*, 110, A12S27, doi:10.1029/2004JA010856.

Forbes, J. M., Bruinsma, S. L., Miyoshi, Y., & Fujiwara, H. 2008, *Geophys. Res. Lett.*, 35, L14802, doi:10.1029/2008GL034075.

Ford, E. A. K., Aruliah, A. L., Griffin, E. M., & McWhirter, I. 2007, *Ann. Geophys.*, 25, 1269.

Fujiwara, H. & Miyoshi, Y. 2006, *Geophys. Res. Lett.*, 33, L20108, doi:10.1029/2006GL027103.

Fujiwara, H. & Miyoshi, Y. 2009, *Earth Planets Space*, 61, 463.

Fuller-Rowell, T. J. & Rees, D. 1980, *J. Atmos. Sci.*, 37, 2545.

Fuller-Rowell, T. J., Akmaev, R. A., Wu, F., Anghel, A., Maruyama, N., Anderson, D. N., Codrescu, M. V., Iredell, M., Moorthi, S., Juang, H.-M., Hou, Y.-T., & Millward, G. 2008, *Geophys. Res. Lett.*, 35, L09808, doi:10.1029/2007GL032911.

Hedin, A. E., Fleming, E. L., Manson, A. H., Schmidlin, F. J., Avery, S. K., Clark, R. R., Franke, S. J., Fraser, G. J., Tsuda, T., Vial, F., & Vincent, R. A. 1996, *J. Atmos. Terr. Phys.* 58, 1421.

Ishii, M., Oyama, S., Nozawa, S., Fujii, R., Sagawa, E., Watari, S., & Shinagawa, H. 1999, *Earth Planets Space.*, 51, 833.

Jin, H., Miyoshi, Y., Fujiwara, H., & Shinagawa, H. 2008, *J. Geophys. Res.*, 113, A09307, doi:10.1029/2008JA013301.

Kanamitsu, M., Tada, K., Kudo, T., Sato, N., & Isa, S. 1983, *J. Meteor. Soc. Japan*, 61, 812.

King-Hele, D. G. 1959, *Nature*, 183, 1224.

King-Hele, D. G. 1987, *Satellite Orbits in an Atmosphere: Theory and application*, Springer, p. 304.

Liu, H., Luhr, H., Henize, V., & Kohler, W. 2005, *J. Geophys. Res.*, 110, A04301, doi:10.1029/2004JA010741.

Miyahara, S., Yoshida, Y., and Miyoshi, Y. 1993, *J. Atmos. Terr. Phys.*, 55, 1039.

Miyoshi, Y. 1999, *Earth Planets Space*, 51, 763.

Miyoshi, Y., & Fujiwara, H. 2003, *Geophys. Res. Lett.*, 30, 1789, doi:10.1029/2003GL017695.

Miyoshi, Y., & Fujiwara, H. 2006, *J. Geophys. Res.*, 111, D14108, doi:10.1029/2005JD006993.

Miyoshi, Y., Fujiwara, H., Forbes, J. M., & Bruinsma, S. L. 2009, *J. Geophys. Res.*, 114, A07303, doi:10.1029/2009JA014110.

Nozawa, S., & Brekke, A. 1995, *J. Geophys. Res.*, 100, 14717.

Picone, J. M., Hedin, A. E., Drob, D. P., & Aikin, A. C. 2002, *J. Geophys. Res.*, 107(A12), 1468, doi:10.1029/2002JA009430.

Prölss, G. W. 1982, *J. Geophys. Res.*, 87, 5260.

Richards, P. G., Fennelly, J. A., & Torr, D. G. 1994, *J. Geophys. Res.*, 99, 8981.

Roble, R. G.. 2000, *AGU monograph*, 123, 53.
Shiokawa, K., Kadota, T., Otsuka, Y., Ogawa, T., Nakamura, T., & Fukao, S. 2003, *Earth Planets Space*, 55, 271.
Sutton, E. K., Forbes, J. M., Nerem, R. S., & Woods, T. N. 2006, *Geophys. Res. Lett.*, 33, L22101, doi:10.1029/2006GL027737.
Toth, G., De Zeeuw, D. L., Gombosi, T. I., Manchester, W. B., Ridley, A. J., Sokolov, I. V., & Roussev, I. I. 2007, *Space Weather*, 5, S06003, doi:10.1029/2006SW000272.
Wang, W., Wiltberger, M., Burns, A. G., Solomon, S. C., Killeen, T. L., Maruyama, N., & Lyon, J. G. 2004, *J. Atmos. Solar-Terr. Phys.*, 66/15–16, 1425.